

## **EXPERIMENT AND NUMERICAL SIMULATIONS ON SFR CORE-CATCHER SAFETY ANALYSIS AFTER RELOCATION OF CORIUM**

X. GAUS-LIU<sup>1</sup>, B. BIGOT<sup>2</sup>, C. JOURNEAU<sup>2</sup>, F. PAYOT<sup>2</sup>, T. CRON<sup>1</sup>, R. CLAVIER<sup>2</sup>, M. Peybernes<sup>2</sup>, P. E. ANGELI<sup>3</sup>, B. FLUHRER<sup>1</sup>

<sup>1</sup> Karlsruhe Institute of Technology (KIT), Eggenstein-Leopoldshafen, Germany

<sup>2</sup> CEA Cadarache, Saint Paul Lez Durance Cedex, France

<sup>3</sup> CEA Paris-Saclay, France

Email contact of corresponding author: xiaoyang.gaus-liu@kit.edu

### **Abstract**

In-vessel core catcher is a safety design feature of European type Sodium-Cooled Fast Reactor (ESFR) to guarantee the reactor integrity during a postulated core-melt accident. The core catcher has the function to collect the relocated melt derived from the upper core area and to prevent local thermal attack of melt on the reactor vessel. The thermodynamics of the melt with decay heat and its heat transfer at the core catcher boundaries will be studied experimentally at KIT and numerically at CEA.

A new large-scale 3D vessel, ESFR-LIVE, is built at KIT imitating the geometry of the core-catcher in a diameter scale of 1:6. The lower part of the vessel is a truncated cone and the upper part is a cylinder. All the vessel boundaries are enclosed in a water-cooled vessel and the melt surface was cooled by a cooling lid. The decay power is simulated by four planes of resistance heater with a total power up to 86 kW. The melt pool geometry can be varied by shifting the upper lid and/or crust-building at the bottom. Measurable parameters are bulk temperature and boundary temperature of the melt, 3D vessel wall temperatures and heat flux. The simulant of oxide melt is eutectic NaNO<sub>3</sub>-KNO<sub>3</sub> mixture allowing operation temperature up to 400 °C. Results of similarity comparisons indicate that Rayleigh number (Ra) of the experiment is comparable to the reactor case, thus the experiment can capture both general heat transfer characteristics and local heat transfer details.

Computational Fluid Dynamics (CFD) pre-calculations with TrioCFD code is performed for designed test conditions. The simulations use High Performance Computing on ten million of mesh nodes. The numerical work selects Large Eddy Simulation (LES) models regarding the high Rayleigh number. A mesh resolution analysis is performed, followed by a parametric study predicting the melt velocity, temperature and heat fluxes.

### 1. INTRODUCTION

The study bears one of the aim of EU H2020 ESFR-SMART project [1] to improve the understanding and provide quantitative estimation on the heat transfer of corium after relocation in a SFR-core catcher to ensure the safety criterial in the long term. Although many previous studies have been reported on the heat transfer behaviour on a cavity filled with corium and cooled at all boundaries, such as the study of the PWR/VVER in-vessel melt retention at the reactor lower head [2-5], the results of these studies cannot be transferred directly to the core-catcher heat transfer due to the difference in the geometry, which effects the turbulent flow extensively. Comparing to the reactor lower head in spherical or torispherical geometry, the corium pool in core catcher is very shallow, which has limited sidewall area for the heat transfer. For the overall heat transfer, understanding both the heat transfer coefficients at the upper surface and at the lateral wall are important, since the balance of the two heat rates influences the lateral heat flux. For the case of localized heat flux, critical hotspot on the vessel wall should be identified for the design of robust core-catcher wall structure. To provide reliable data to limit above uncertainties, a new facility with core-catcher cavity character is constructed at KIT and will be commissioned in the summer 2021. The new facility will provide local heat flux and the general heat transfer ratio of upper surface to sidewall, the bulk pool temperatures, pool boundary temperatures, wall inner surface and outer surface temperatures. The great advantage of the experiment is that the corium pool geometry and the pool height are variable, and the power input density is much higher than the earlier facility LIVE-3D [6]. This study provides the technique details of the facility, similarity analysis and three pre-test calculations.

## 2. TEST FACILITY

### 2.1. Test vessel and cooling system

The new-built ESFR- LIVE test vessel is integrated in the LIVE experimental platform [5] and is located at the same position as the former LIVE3D test, see Fig. 1. Besides the test vessel, the platform includes logistic of melt preparation, pouring and recycling, cooling water supply, power supply and control, and data acquisition system. An external heating furnace is used for the melt preparation, pouring, extraction and storage. The experiment begins generally with the melt pour from the heating furnace via a pouring spout into the test vessel and is terminated by melt extraction from the test vessel back to the heating furnace.

The ESFR-LIVE test vessel simulates the typical tray geometry of an in-vessel SFR core catcher, whose cavity has a geometry of truncated cone in the lower part, and cylinder in the upper part. The inner diameter of the upper cylinder is 1 m, and thus is in 1:6 length scale. The total height of the test vessel inner cavity is 0.38 m, and provides the flexibility of the pool height and the position of the cooling lid. The truncated cone is 0.08 m in height, thus corresponding to 1:1 scale of the prototype geometry. The inclined sidewall is  $20^\circ$  to the horizontal orientation. The test vessel is made of stainless steel and in 0.015 m thickness. The external cooling of liquid Na is simulated by water in ground temperature. A cooling vessel encloses the test vessel and creates a cooling channel of 0.06 m in width. Cooling water flows in at the bottom and flows out at four outlets at the vessel upper edge. The flow rate is controlled to enable a certain difference between the water inlet and outlet temperature.

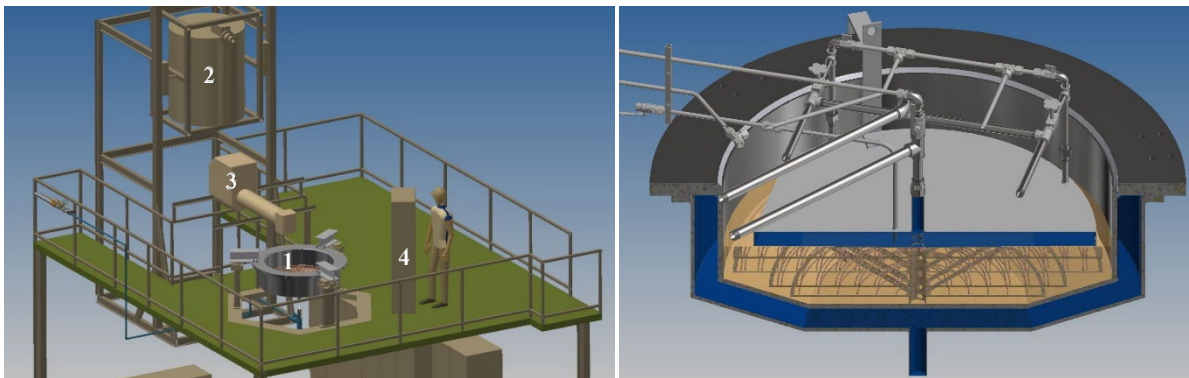


Fig. 1 Left: LIVE experimental platform with ESFR-LIVE facility. 1- ESFR test vessel, 2 - heating furnace for melt preparation, 3 - pouring spout, 4 - instrumentation board. Right: ESFR-LIVE test vessel with all boundary cooling system.

The top surface of the vessel can be either cooled with a water-cooled lid or be insulated by covering an insulation lid, see Fig. 1. The upper cooling lid is a water-cooled container, which has four inlets at the periphery and one outlet at the central of the lid. The cooling lid position is flexible and can be placed from the bottom part of the cylindrical part upwards. The direct contact between the melt surface and the cooling lid is controlled regularly.

### 2.2. Heating system

Four planes of resistance heating element are designed to simulate the decay heat of the corium, which are named HE1 to HE4 from the bottom upwards, as shown in Fig. 2. Two planes are located in the truncated cone (HE1 and HE2) and the other two are located in the cylindrical part (HE3 and HE4). The upper two heating planes can be removed individually to enable different pool heights at the top boundary. The total heating power can reach 86.5 kW. The cross diameter of the heating cable is 4 mm, and the cables are formed spirally with even distance. Some heating planes are in duplex winding to enable high power inputs. All the heating planes can be controlled individually and thus variations of the height of the truncated part is possible by shutdown the one or two of the lower heaters. Correspondingly, bottom crust grows upwards till the level of the lowest heater in operation.

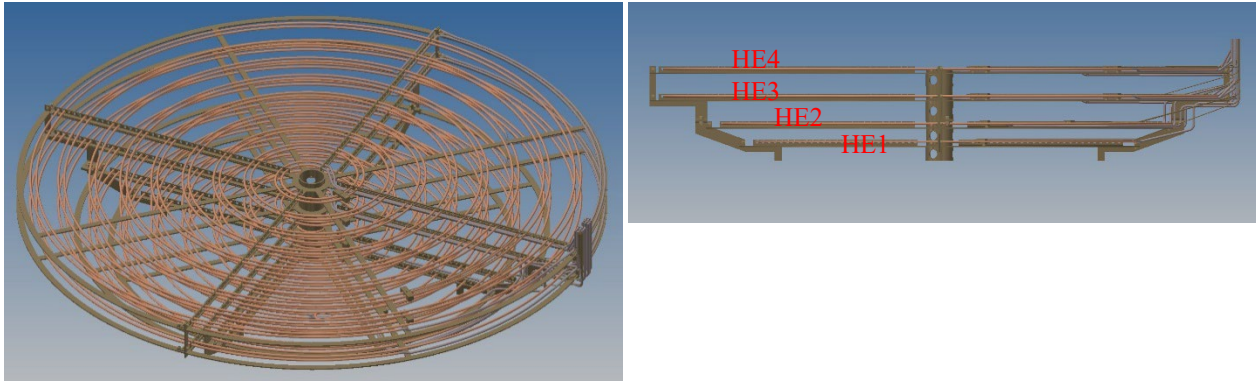


Fig. 2. Heating system of ESFR-LIVE

### 2.3. Instrumentations and simulant material

The instrumentation of the ESFR-LIVE includes:

- 44 pairs of thermocouples (TCs) measuring vessel wall inner temperature (IT) and outer surface temperature (OT) on 4 azimuth axils. At each axil 11 pairs TC are arranged in the order of 3 pairs at the bottom plate, 3 pairs at the truncated cone vessel wall and 5 pairs at the cylindrical vessel wall. Local heat fluxes can be obtained based on the temperature difference between a IT/OT pair at one position.
- 49 TCs measuring melt temperature (MT) are arranged in the angle of  $45^\circ - 225^\circ$ , as shown in Fig. 3. The symmetrical arrangement of the MTs under the heating planes are used for the examination of the symmetricity of 3-D thermo-hydraulics of the melt pool, and the additional MT planes and the wall-near TCs at azimuth  $45^\circ$  can provide more details of the crust positions.
- Instrumentation at the top cooling lid: three thermocouple trees (DCT) and four surface temperature TCs (DIT) are arranged at the bottom plate of the cooling lid to measure the interface temperature at the crust / lid and the top boundary temperature.
- Cooling water flow rate, inlet temperature and outlet temperature for the estimation of the integral waterside heat removal rate at the vessel wall and at the melt surface.
- Weight change of the vessel.
- Temperature upper limit control with automatic shutdown for all heaters.

The data signals are recorded with the Labview program of National Instruments. The simulant material of the corium melt is the eutectic  $\text{NaNO}_3\text{-KNO}_3$  mixture with the melting temperature of  $220^\circ\text{C}$ . The low melting temperature enables a large super heat range between  $220^\circ\text{C}$  and  $400^\circ\text{C}$ . In addition, its simple non-mushy-zone solidification character simplifies physical modelling.

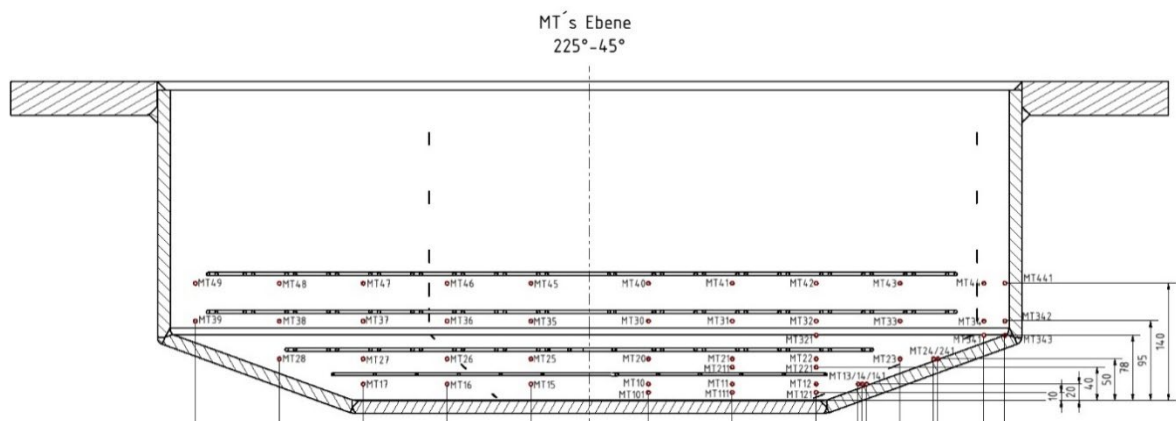


FIG. 3. TC positions for melt temperature measurement

### 3. TEST DEFINITION AND SIMILARITY ANALYSIS

Two test series are planned: one series with a pool volume to the highest heater, the other series with the melt only filling the truncated cone part. In the first test series, the lower part of melt pool geometry will be varied by shutdown the two lower heaters HE1 and HE2 one by one, as shown in Table 1. The liquid melt below the operating heaters will be solidified due to the bottom cooling and very low downward heat transfer rate. Several power levels will be performed for each of the pool geometry to obtain the heat transfer characteristic under a large range of Ra and heat flux. The test conditions of the second test series will be detailed after gathering the experience of the first test series.

TABLE 1. TEST CONDITIONS IN THE FIRST TEST SERIES EL-1.

Melt pool configuration	EL-1A	EL-1B	EL-LC
Heaters in operation	HE1 - HE4	HE2 - HE4	HE3 - HE4
Height in truncated cone part, m	0.08	0.05	0
Height in cylinder part, m	0.1	0.1	0.1
Total pool height, m	0.18	0.15	0.1
Number of power levels	4	3	3

The similarity of the geometry, thermophysical properties and thermodynamic of the ESFR-LIVE experiments are compared with the reactor case to verify the applicability of the experimental result. In Table 2 comparisons are given on the comparison in geometry, material properties and thermodynamic similarities. The thermodynamic parameters of ESFR-LIVE are estimated for the power of 67 kW in the case of EL-1A (Table 1). Three heat transfer calculation methods are carried out: a) applying external Ra ( $Ra_{ex}$ ) by suiting the boundary temperature, performed by KIT, b) applying internal Ra ( $Ra_i$ ) by applying the power input density, performed by CEA and c) numerical calculation applying Trio-CFD and using a LES model, performed by CEA, which will be introduced in the following section. For the numerical results, only the lateral heat flux at the cylindrical wall. is shown here.

The corium in the reactor case is assumed as  $UO_2$  with the properties given by Kim [7] and Harding [8]. The properties of the eutectic nitrate melt are referred in [9]. The equations of  $Ra_{ex}$  and internal  $Ra_i$  are given in Eq. (1) and Eq. (2) respectively. The ESFR-LIVE melt pool has the same height as reactor corium pool. The radius/height aspect ratio of the experiment is 10 in ESFR-LIVE, which is large enough to neglect the lateral boundary effect on the upwards heat transfer. The thermodynamic similarity, characterised by both  $Ra_i$  and  $Ra_{ex}$  are in the same order as the reactor case. Three sets of heat flux are presented, which show the similar trend of heat flux ratio in top surface to lateral surface but in different values to some extent.

The heat transfer calculation undergoes certain uncertainty due to the selection of the Nu~Ra correlations. For the method a), which applies  $Ra_{ex}$ , the Globe & Dropkin correlation [10] in Eq. (3) is used for the upper surface heat transfer, and the Churchill & Chu correlation [11] in Eq. (4) is used is for the sidewall heat transfer. For the method b), whereas the  $Ra_i$  is applied, Steinberner and Reinecke Correlations for a rectangular cavity with an aspect ratio  $A=1$  are applied, as given in Eq. (5) for the upper surface heat transfer and in Eq. (6) for sidewall heat transfer [12].

TABLE 2. SIMILARITY STUDIES AND HEAT FLUX PREDICTIONS

	Reactor / Oxid melt	ESFR-LIVE	Scale experiment/reactor
<b>Cavity geometry</b>			
$D$ , Diameter, m	6	1	1:6
$D_h$ , Height /Characteristic length, m	0.18	0.18	1:18
$A$ , Aspect ratio: diameter / height, -	60	10	1:6
<b>Material properties</b>			
$\rho$ , Density, kg/ m <sup>3</sup>	8703 [7]	1747	0.2
$\mu$ , Dynamic viscosity, mPa·S	4.035 [7]	3.102	0.77
$\lambda$ , Thermal conductivity, W/(mK)	3.52 [7]	0.459	0.13
$\beta$ , Thermal expansion rate, 1/K	$1.05 \cdot 10^{-4}$	$3.81 \cdot 10^{-4}$	3.65:1
$C_p$ , Thermal capacity, J/kg/K	485 [8]	1492	3.08:1
$Pr$	0.556	10.092	18.2:1
<b>Thermodynamics and Heat transfer</b>			
Superheat, K	327	70	
Power input, kW	30711	67	0.002
$Ra_i$	$3.37 \cdot 10^{11}$	$9.18 \cdot 10^{11}$	2.72
$Ra_{ex}$	$2.59 \cdot 10^9$	$2.50 \cdot 10^9$	0.97
$q_{lat\_Ra\_i}$ , W/m <sup>2</sup>		50.3	
$q_{up\_Ra\_i}$ , W/m <sup>2</sup>		37	
$q_{lat\_Ra}$ , W/m <sup>2</sup>	1330	36.9	0.028
$q_{up\_Ra\_ex}$ , W/m <sup>2</sup>	729	24.8	0.034
$q_{lat\_up\_num}$ , W/m <sup>2</sup>		78.6	
$q_{up\_num}$ , W/m <sup>2</sup>		33.5	

$$Ra_{ex} = Gr \cdot Pr = \frac{g\beta\Delta TL^3}{\alpha\nu} \quad (1)$$

$$Ra_i = Gr \cdot Pr \cdot Da = \frac{g\beta\dot{q}L^5}{\alpha\lambda\nu} \quad (2)$$

$$Nu_{up} = 0.069Ra_{ex}^{1/3} Pr^{0.074}, Ra_{ex}: 3 \cdot 10^5 - 7 \cdot 10^9; Pr: 0.02-8750 \quad (3)$$

$$Nu_{sd} = \left\{ 0.825 + \frac{0.387 Ra_{ex}^{1/6}}{\left[ 1 + \left( \frac{0.492}{Pr} \right)^{9/16} \right]^{2/7}} \right\}^2, Ra_{ex} < 10^{12}, all Pr \quad (4)$$

$$Nu_{up} = 0.345Ra_i^{0.233}, Ra_i: 5 \cdot 10^{12} \sim 3 \cdot 10^{13}, Pr \sim 7 \quad (5)$$

$$Nu_{sd} = 0.85Ra_i^{0.19}, Ra_i: 5 \cdot 10^{12} \sim 3 \cdot 10^{13}, Pr \sim 7 \quad (6)$$

The applicability of the three methods on the heat transfer calculation of the corium in a SFR core catcher will be therefore verified by the experiment result. All the methods show that the lateral heat flux is considerable higher than the top surface heat flux. However, due to the large area at the upper surface the upwards heat transfer will considerably contribute the overall heat removal, and reduce the bulk temperature, which in return reduces effectively the thermal load on the lateral wall.

#### 4. NUMERICAL CALCULATION

##### 4.1. Model description

Numerical simulation with the TrioCFD code [13] was used for the pre-calculation, by which the incompressible Navier-Stokes equation, under Boussinesq approximation, and the heat equation were solved. The solution was

to apply a LES (Large-Eddy-Simulation) turbulence model to describe the turbulence scales with sizes equal to or less than the Taylor scale. The Taylor scale characterizes a scale below which the viscous effects dominate the inertial effects. The LES model named WALE (Wall-Adapting Local Eddy viscosity) was used in the computations. A non-uniform meshing was built with mesh sizes equal to the local Taylor scale of the flow. The 3D meshing consists of around  $9.1 \times 10^6$  meshes. An illustration of this meshing is presented in Fig. 4 with a cross section.

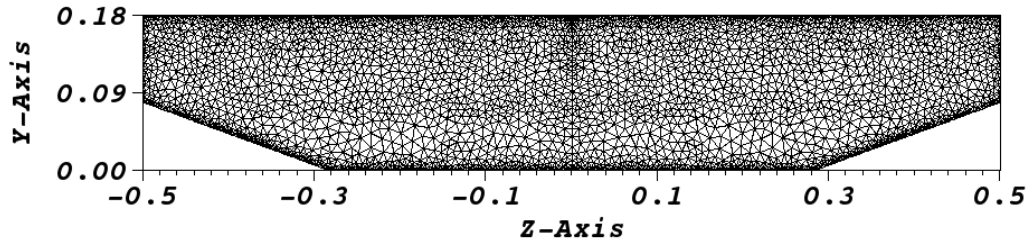


FIG. 4. Cross section of the computational domain of the device consists of  $9.1 \times 10^6$  meshes with mesh sizes equal to Taylor local scales of the turbulent flow.

In order to ensure that the meshing is sufficiently fine, the ratio between the local Taylor scale and the meshes size was computed and illustrated in Fig. 5. With a cross section of the computational domain. This ratio shows that the numerical computation is well resolved (for the meshing) with meshes sizes mainly lower than Taylor scale (calculated during steady state). Figure 4 shows the number of meshes distribution for this ratio indicating that only 4.2 % of the meshes over  $9.1 \cdot 10^6$  is not resolved (with a ratio between 0.1 and 1). These results show a suitable meshing resolution.

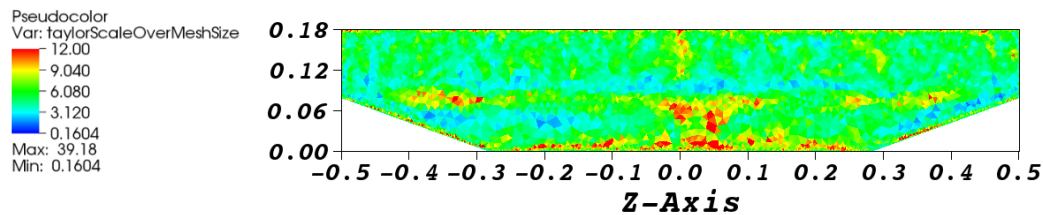


Fig. 5. cross section of the computational domain for the ratio between the local Taylor scale and mesh size.

Fig. 6 presents the 3D geometry of the experimental device (previously meshed). The device is made up of “lower” (blue), “upper” (yellow) and two lateral surfaces: “lateral1” (green) for the lower truncated cone part and “lateral2” (red) for the upper cylindrical part.

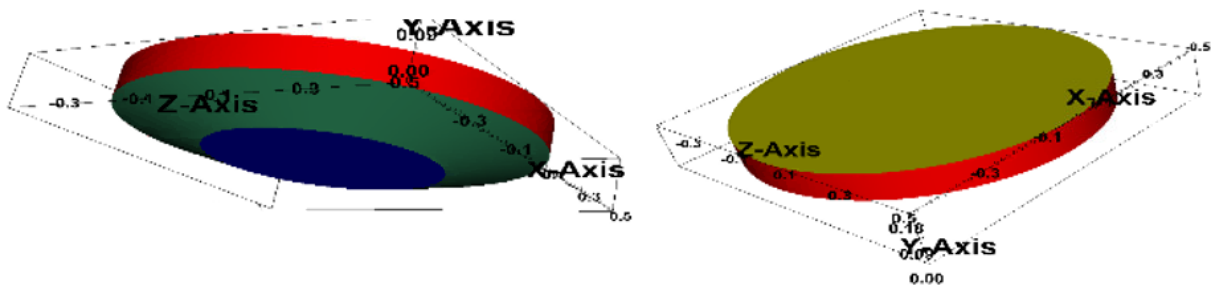


Fig. 6. Experimental device obtained from computations with TrioCFD code and made up of four surfaces : “lower” (blue), “upper” (yellow), “lateral1” (green) and “lateral2” (red).

#### 4.2. Pre-test results of the numerical simulation

Fig. 7 shows the velocity and temperature fields in a stationary statistically regime and statistically averaged in this regime for a power of 53 kW. The results for a power of 67 kW have the similar distributions. A comparison of average heat flux for 53 KW and 67 kW is given in Table 3. Flow presents convective vortices

characteristics to a natural Rayleigh-Bernard convection sustained by internal volumetric power density and with an external wall coolant. The temperature field presents a stratification with two distinct zones due to the flow density variation (due to a thermal dilatation) in the gravity field. The lower and “lateral1” surface temperatures are lower than the upper and “lateral2” ones (493 K against 525 K).

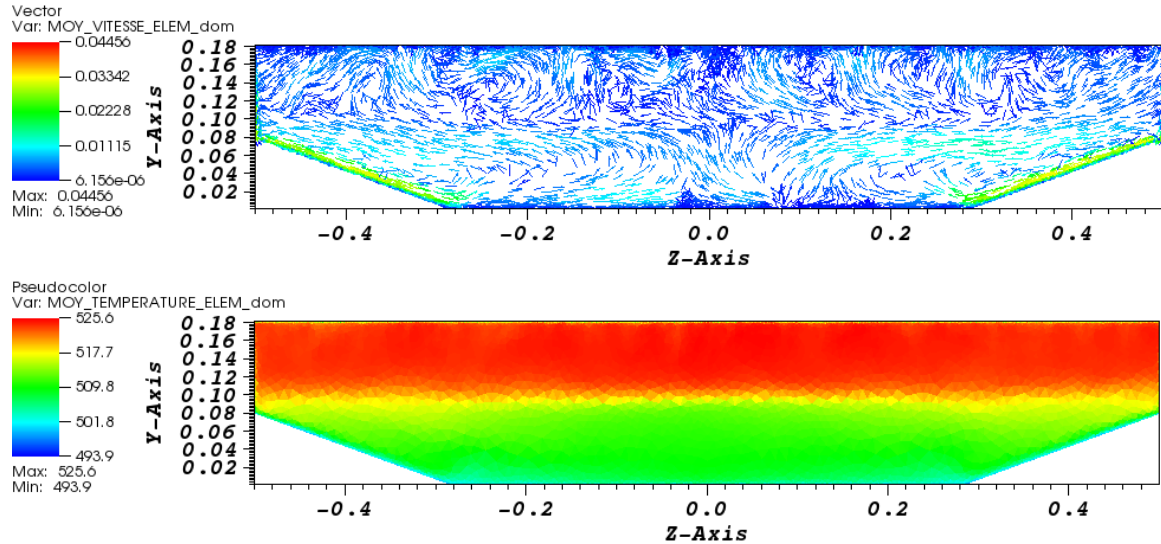


Fig. 7. Cross-section of the velocity (top) and temperature (bottom) fields in the device during the stationary statistically regime and statistically averaged in this regime.

TABLE 3. HEAT FLUXES RECEIVED BY THE FOUR SURFACES FOR TWO INTERNAL VOLUMETRIC POWER RATES.

Internal volumetric power density (kW)	« Lower » average flux (kW/ m <sup>2</sup> )	« Upper » average flux » (kW/ m <sup>2</sup> )	« Lateral1 » average flux (kW/ m <sup>2</sup> )	« Lateral2 » average flux (kW/m <sup>2</sup> )
67	3.4	33.5	26.7	78.6
53	2.8	27.2	21.4	64.6

## 5. SUMMARY

A new facility in form of a SFR- core catcher is built to provide reliable data for the understanding of heat transfer and ablation behaviour of a corium pool after its relocation in a SFR in-vessel core-catcher. The thermodynamic and material features of the experiment are very similar as those of an oxide corium pool. The flexible design and high power input enable a wide range of test conditions. Two series of experiments will be performed in summer 2021. The paper presents the results of three pre-test calculations, which have shown similar trends but different values on the heat fluxes at the upper surface and lateral surface. Experimental results are expected to verify empirical correlations and validate the numerical study.

## ACKNOWLEDGEMENTS

The experimental study is financially supported by the EU-H2020 Project ESFR-SMART with the Project Number 754501 and Germany federal government Helmholtz Society. The numerical work was granted access to the HPC resources of the CEA's Very Large Computing Centre (TGCC) under the allocation 2021 A0012A07691 made by GENCI.

**REFERENCES**

- [1] EU H2020 ESFR-SMART Project. Available from: <http://esfr-smart.eu/>.
- [2] Theofanou, T.G. and S. Angelini, Natural convection for in-vessel retention at prototypic Rayleigh numbers. *Nuclear Engineering and Design*, 200, (2000), p. 1-9.
- [3] Bonnet, J.M. and J.M. Seiler, Thermal Hydraulic Phenomena in Corium Pools: the BALI Experiment, in ICONE-7. Tokyo, Japan. p. ICONE-7057, (1999).
- [4] Helle, M., O. Kymäläinen, and H. Tuomisto, EXPERIMENTAL COPO II DATA ON NATURAL CONVECTION IN HOMOGENOUS AND STRATIFIED POOLS, in Ninth International Topical Meeting on Nuclear Reactor Thermal Hydraulics (NURETH-9), San Francisco, USA (1999).
- [5] Gaus-Liu, X., et al., Core melt solidification characteristics in RPV lower head. Experimental results from live-tests, in Proc.of the 17th Internat.Conf.on Nuclear Engineering (ICONE-17), Bruxelles, ICONE17-75450, (2009).
- [6] Gaus-Liu, X., et al., LIVE L4 and LIVE L5L experiments on melt pool and crust behaviour in the RPV lower head, in 14th Internat.Topical Meeting on Nuclear Reactor Thermalhydraulics (NURETH-14), Toronto, CDN, September 25-30, Proc.on CD-ROM NURETH14-26 Toronto, (2011).
- [7] Kim, W.K., J.H. Shim, and M. Kaviani, Thermophysical properties of liquid UO<sub>2</sub>, ZrO<sub>2</sub> and corium by molecular dynamics and predictive models. *Journal of Nuclear Materials* (2017), 491: p. 126-137.
- [8] J.H. Harding, D.G.M., P.E. Potter, Thermalphysical and thermalchemical properties of reactor material, 1989.
- [9] Janz, G.J., et al., Physical properties data complications relevant to Energy storage II. Molten salts: Data on single and multi-component salt systems, in NSRDS-NBS 61, Part II. National Bureau of Standards, U.S. Department of Commerce: New Work, 1979.
- [10] Globe, S. and D. Dropkin, Natural-Convection Heat Transfer in Liquids Confined by Two Horizontal Plates and Heated From Below. *Journal of Heat Transfer*, 81, (1959): p. 24-28.
- [11] Churchill, S.W. and H.H.S. Chu, Correlating Equations for Laminar and Turbulent Free Convection from a Vertical Plate. *International Journal of Heat and Mass Transfer*, 18, (1975): p. 1323-1329.
- [12] Nourgaliev, R.R., T.N. Dinh, and B.R. Sehgal, Effect of fluid Prandtl number on heat transfer characteristics in internally heated liquid pools with Rayleigh numbers up to 1012. *Nuclear Engineering and Design*, 169(1) (1997): p. 165-184,
- [13] Code TrioCFD, CEA. Available from: <http://www-trio-u.cea.fr>.